Deformation Measurements by Digital Image Correlation: Implementation of a Second-order Displacement Gradient

by H. Lu and P. D. Cary

ABSTRACT—This paper outlines the procedure for refining the digital image correlation (DIC) method by implementing a second-order approximation of the displacement gradients. The second-order approximation allows the DIC method to directly measure both the first- and second-order displacement gradients resulting from nonlinear deformation. Thirteen unknown parameters, consisting of the components of displacement, the first- and second-order displacement gradients and the gray-scale value offset, are determined through optimization of a correlation coefficient. The previous DIC method assumes that the local deformation in a subset of pixels is represented by a first-order Taylor series approximation for the displacement gradient terms, so actual deformations consisting of higher order displacement gradients tend to distort the infinitesimal strain measurements. By refining the method to measure both the first- and second-order displacement gradients, more accurate strain measurements can be achieved in large-deformation situations where second-order deformations are also present. In most cases, the new refinements allow the DIC method to maintain an accuracy of ±0.0002 for the first-order displacement gradients and to reach ±0.0002 per pixel for the second-order displacement gradients.

KEY WORDS—Computer vision/digital image processing, data reductions, electronic recording interferometry

Introduction

Digital image correlation (DIC) has become an accepted method for measuring the surface displacements and displacement gradients in materials under deformation. Originally proposed by a group of researchers at the University of South Carolina,[1–5] this method has been refined and extended by others. Vendroux and Knauss[6–8] and Vendroux[9] refined and optimized the basic algorithms used for two-dimensional DIC. These refinements were made primarily in three different areas. A large-deformation description was used to improve the accuracy of the measurements of infinitesimal strains by eliminating the effects of rigid deformations. A least squares correlation coefficient was proposed in place of the commonly used cross-correlation coefficient for measuring the correlation of the deformation mapping of the reference image to the deformed image. An approximated Hessian matrix was used in the Newton-Raphson minimization algorithm to speed up the optimization looping and provided for more robust convergence characteristics.

The DIC method relies on the existence of a distinct gray-scale pattern in a region composed of a subset of pixels around a location where deformations are computed. DIC is performed between a subset in the reference configuration and its image in the deformed configuration. The size of a typical subset region is somewhere between 10×10 pixels and 41×41 pixels. Previous algorithms[1–9] assumed a first-order, linear approximation of the deformation mapping. This approximation holds reasonably well when the size of the subset is small, on the order of a few pixels at each side of a square; however, a distinct gray-scale pattern might not exist in this small region, and thus it is difficult to perform image correlation to find the deformations. A subset region of a relatively large size, on the order of tens of pixels at each side of a square, could possess a distinct gray-scale pattern necessary for image correlation; however, linear deformation mapping in the relatively large subset region might not be appropriate, and instead the researcher must use higher order deformation mapping.

In this paper, we use the DIC method to study relatively large two-dimensional deformation. In general, as the size of the subset region becomes larger and the magnitudes of the displacement gradients increase, the likelihood of the displacement field in the subset region remaining linear can be reduced. Therefore, the variations induced by these higher order displacement gradients must be taken into account. Accounting for these higher order gradients prevents them from clouding the infinitesimal strain measurements, which depend only on the first-order partial derivatives of displacements. In cases of relatively large deformation where second-order deformations are also present, previous algorithms[1–9] at best tended to average in the higher order deformation and at worst would not satisfactorily converge because of the inability to map the deformation. The new implementation presented in this paper incorporates a second-order approximation of the deformation mapping. This will allow a more accurate determination of the deformation parameters directly related to the strain components by determining and accounting for the effect of the second-order mapping parameters. The second-order Taylor series approximation of the displacement field will allow the DIC method to directly measure displacements, first-order displacement gradients and second-order displacement gradients present in the subset region. While this higher order approximation does

H. Lu (SEM Member) is an Assistant Professor, School of Mechanical and Aerospace Engineering, Oklahoma State University, Stillwater, OK 74078. P. D. Cary is an Engineer, Cessna Aircraft Company, Wichita, KS 67215.

Original manuscript submitted: October 19, 1999.
Final manuscript received: August 1, 2000.

provide a better measurement of infinitesimal strain in large-deformation situations, it still does not measure exactly all the nonlinear characteristics present in large deformations.

Digital Image Correlation Using Second-order Approximation

In general, the DIC method is performed between two images. One is the reference or undeformed image, and the other is the deformed image. Typically, a grid of nodes is located in the reference image, and the deformation mapping is calculated at each of these nodes. The fundamental level of the calculation is at the node level, so the following development of the algorithm is for each node.

Displacement Mapping

Consider a two-dimensional deformation. A subset of points around a node is mapped from the reference image to the deformed image. Each of these subset points is located in the reference image at (x, y) and is mapped to the deformed image at location $(\tilde{x}, \tilde{y})$ using

$$\begin{aligned} \tilde{x} &= x + U(x, y) \\ \tilde{y} &= y + V(x, y), \end{aligned} \tag{1}$$

with U and V being the displacement components of each subset point. The new assumption that U and V can be approximated by a second-order Taylor series expansion around point (x_0, y_0) leads to the mapping functions

$$\begin{aligned} \tilde{x} &= x_0 + U_0 + U_x\Delta x + U_y\Delta y + \frac{1}{2}U_{xx}\Delta x^2 \\ &\quad + \frac{1}{2}U_{yy}\Delta y^2 + U_{xy}\Delta x\Delta y \\ \tilde{y} &= y_0 + V_0 + V_x\Delta x + V_y\Delta y + \frac{1}{2}V_{xx}\Delta x^2 \\ &\quad + \frac{1}{2}V_{yy}\Delta y^2 + V_{xy}\Delta x\Delta y, \end{aligned} \tag{2}$$

where $\Delta x = x - x_0$ and $\Delta y = y - y_0$.

Twelve mapping parameters are introduced in eq (2): U_0 and V_0, the components of the displacement at (x_0, y_0); U_x, V_x, U_y and V_y, the components of the first-order displacement gradient; and U_{xx}, V_{xx}, U_{yy}, V_{yy}, U_{xy} and V_{xy}, the components of the second-order displacement gradient. Figure 1 shows the effects of the first- and second-order derivatives of the displacements on the subset of points around the node being analyzed. From Fig. 1, it can be seen that a much broader range of deformation can be accurately represented from the combination of these 12 parameters.

Bicubic Spline Interpolation

Figure 2 shows an example of a bicubic spline surface[10] that has been interpolated through a set of image pixel gray-scale values. The bicubic spline interpolation implements a third-order polynomial that allows both gray-scale values and C^2 continuous gradients to be determined at any location in the gray-scale image fields. Bicubic spline interpolation is a piecewise interpolation scheme in which a set of coefficients

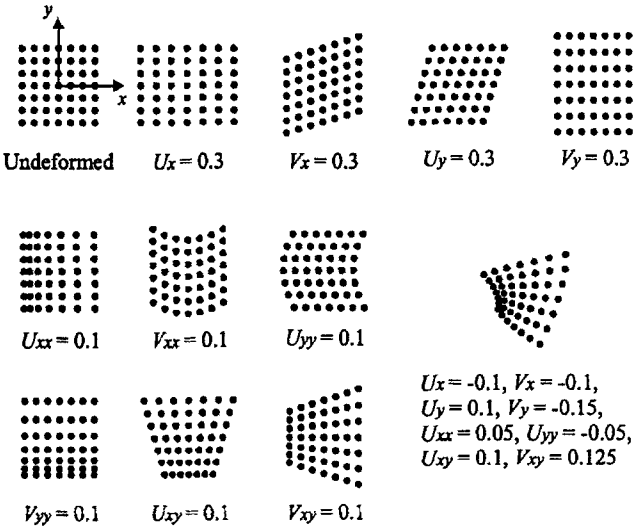

Fig. 1—Effect of displacement gradients on subset points

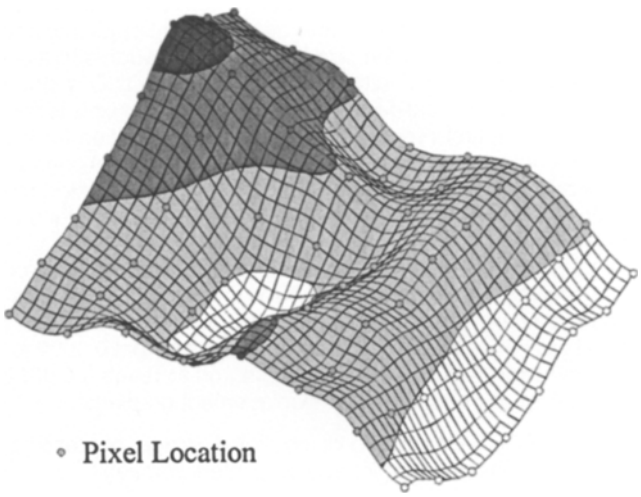

Fig. 2—Bicubic spline interpolation of image gray-scale data

are determined for each rectangular patch. Both the reference and the deformed images are interpolated to allow the nodes to be located anywhere in the image fields. The gray-scale value at any location in the interpolated region of the reference image can be calculated using the bicubic equation

$$g(x, y) = \sum_{m=0}^{3}\sum_{n=0}^{3}\alpha_{mn}x^m y^n. \tag{3}$$

Following Vendroux and Knauss,[7] we introduce the 13th mapping parameter w in the form of a gray-scale value offset of the bicubic spline interpolation for the deformed image. This parameter is introduced to allow us to make the assumption that the gray-scale values g in the reference image are approximately the same as the gray-scale values h in the deformed image. Differences in the brightness of the images could result due to lighting changes between the acquisitions of the two images. The equation for the interpolated deformed image is then

$$h(\tilde{x}, \tilde{y}, \boldsymbol{P}) = \sum_{m=0}^{3}\sum_{n=0}^{3}\beta_{mn}\tilde{x}^m\tilde{y}^n + w. \tag{4}$$

For later simplification, let $\boldsymbol{P}$ represent a vector with all 13 mapping parameters as its components.

Correlation

A least square correlation coefficient[7,11] is used to determine the optimum values for the mapping parameters. Let S represent all the points in the subset, and let S_p represent any single point in the subset. This correlation coefficient is defined as

$$C = \frac{\sum_{S_p \in S}\left\{g(S_p) - h(S_p, \boldsymbol{P})\right\}^2}{\sum_{S_p \in S} g^2(S_p)}. \tag{5}$$

The summations are performed over all the points in the subset region. From the equation, the range of values for C is $[0, \infty)$, where the minimum is reached when the differences between g and h are minimized. The set of $\boldsymbol{P}$ that minimizes the correlation coefficient C is in fact the parameters of the mapping caused by the deformation.

To find the minimum C, the gradient of C must converge to zero, that is,

$$\nabla C = \left(\frac{\partial C}{\partial P_i}\right)_{i=1,13} = \frac{-2}{\sum_{S_p \in S} g^2(S_p)} \tag{6}$$

$$\left\{\sum_{S_p \in S}\left(g(S_p) - h(S_p, \boldsymbol{P})\right)\frac{\partial h(S_p, \boldsymbol{P})}{\partial P_i}\right\}_{i=1,13} = 0.$$

The Newton-Raphson[11] method is used to solve for the roots of eq (6). This method uses an approximate value for the root of a function, then iterates until it converges to the actual roots. In the DIC algorithm, the roots of the gradient of the correlation coefficient ∇C must be found. Therefore, the Newton-Raphson equation would be

$$\left[\nabla\nabla C(\boldsymbol{P}_0)(P - P_0)\right] = -\left[\nabla C(\boldsymbol{P}_0)\right], \tag{7}$$

where $\boldsymbol{P}_0$ is an initial guess of the solution and $\boldsymbol{P}$ is the next iterative approximate solution of eq (6). $\nabla\nabla C(\boldsymbol{P})$ is the second-order gradient of the correlation coefficient, also known as the Hessian matrix. The Hessian matrix of the correlation coefficient can be computed by

$$\nabla\nabla C = \left(\frac{\partial^2 C}{\partial P_i \partial P_j}\right)_{\substack{i=1,13\\ j=1,13}}$$

$$= \left\{\frac{-2}{\sum_{S_p \in S} g^2(S_p)}\sum_{S_p \in S}\left(g(S_p)\right. \right. \tag{8}$$

$$\left. -h(S_p, \boldsymbol{P})\right)\frac{\partial^2 h(S_p, \boldsymbol{P})}{\partial P_i \partial P_j}$$

$$\left. + \frac{2}{\sum_{S_p \in S} g^2(S_p)}\sum_{S_p \in S}\frac{\partial h(S_p, \boldsymbol{P})}{\partial P_i}\frac{\partial h(S_p, \boldsymbol{P})}{\partial P_j}\right\}_{\substack{i=1,13\\ j=1,13}}.$$

Based on the approach proposed by Vendroux and Knauss,[7] we can make an approximation to the Hessian matrix. Because we have included the term w to account for any brightness offsets between the two images being correlated, we can assume that at the solution, $g(x, y) \approx h(x, y, \boldsymbol{P})$. The assumption that the initial trial solution for $\boldsymbol{P}$ is close to the solution leads to the following term:

$$\sum_{S_p \in S}\left(g(S_p) - h(S_p, \boldsymbol{P})\right)\frac{\partial^2 h(S_p, \boldsymbol{P})}{\partial P_i \partial P_j} \approx 0. \tag{9}$$

This leads to an approximate Hessian matrix of the correlation coefficient:

$$\frac{\partial^2 C}{\partial P_i \partial P_j} = \frac{2}{\sum_{S_p \in S} g^2(S_p)}\sum_{S_p \in S}\frac{\partial h(S_p, \boldsymbol{P})}{\partial P_i}\frac{\partial h(S_p, \boldsymbol{P})}{\partial P_j}. \tag{10}$$

The derivatives of the gray-scale values with respect to the mapping parameters are functions of both the displacement mapping and the bicubic interpolation of the deformed image pixel data. These partial derivatives can be evaluated using the chain rule

$$\frac{\partial h(S_p, \boldsymbol{P})}{\partial P_i} = \frac{\partial h(\tilde{x}, \tilde{y}, \boldsymbol{P})}{\partial \tilde{x}} \cdot \frac{\partial \tilde{x}(S_p)}{\partial P_i} + \frac{\partial h(\tilde{x}, \tilde{y}, \boldsymbol{P})}{\partial \tilde{y}} \cdot \frac{\partial \tilde{y}(S_p)}{\partial P_i} + \frac{\partial h(\tilde{x}, \tilde{y}, \boldsymbol{P})}{\partial P_i}. \tag{11}$$

The equations for calculating the 13 gradient terms for $\frac{\partial h(S_p, \boldsymbol{P})}{\partial P_i}$ for each point S_p are as follows:

$$\frac{\partial h}{\partial U} = \frac{\partial h}{\partial \tilde{x}} \qquad \frac{\partial h}{\partial V} = \frac{\partial h}{\partial \tilde{y}}$$

$$\frac{\partial h}{\partial U_x} = \frac{\partial h}{\partial \tilde{x}}\Delta x \qquad \frac{\partial h}{\partial V_x} = \frac{\partial h}{\partial \tilde{y}}\Delta x$$

$$\frac{\partial h}{\partial U_y} = \frac{\partial h}{\partial \tilde{x}}\Delta y \qquad \frac{\partial h}{\partial V_y} = \frac{\partial h}{\partial \tilde{y}}\Delta y$$

$$\frac{\partial h}{\partial U_{xx}} = \frac{1}{2}\frac{\partial h}{\partial \tilde{x}}\Delta x^2 \qquad \frac{\partial h}{\partial V_{xx}} = \frac{1}{2}\frac{\partial h}{\partial \tilde{y}}\Delta y^2 \tag{12}$$

$$\frac{\partial h}{\partial U_{yy}} = \frac{1}{2}\frac{\partial h}{\partial \tilde{x}}\Delta y^2 \qquad \frac{\partial h}{\partial V_{yy}} = \frac{1}{2}\frac{\partial h}{\partial \tilde{y}}\Delta y^2$$

$$\frac{\partial h}{\partial U_{xy}} = \frac{\partial h}{\partial \tilde{x}}\Delta x\Delta y \qquad \frac{\partial h}{\partial V_{xy}} = \frac{\partial h}{\partial \tilde{y}}\Delta x\Delta y \qquad \frac{\partial h}{\partial w} = 1.$$

The $\frac{\partial h}{\partial \tilde{x}}$ and $\frac{\partial h}{\partial \tilde{y}}$ terms of these partial derivatives are the gradients of the bicubic spline interpolating polynomial from the deformed image, where

$$\begin{aligned}\frac{\partial h}{\partial \tilde{x}} &= \beta_{10} + \beta_{11}\tilde{y} + \beta_{12}\tilde{y}^2 + \beta_{13}\tilde{y}^3 \\ &+ 2\beta_{20}\tilde{x} + 2\beta_{21}\tilde{x}\tilde{y} + 2\beta_{22}\tilde{x}\tilde{y}^2 + 2\beta_{23}\tilde{x}\tilde{y}^3 \\ &+ 3\beta_{30}\tilde{x}^2 + 3\beta_{31}\tilde{x}^2\tilde{y} + 3\beta_{32}\tilde{x}^2\tilde{y}^2 + 3\beta_{33}\tilde{x}^2\tilde{y}^3\end{aligned} \tag{13}$$

and

$$\begin{aligned}\frac{\partial h}{\partial \tilde{y}} &= \beta_{01} + 2\beta_{02}\tilde{y} + 3\beta_{03}\tilde{y}^2 \\ &+ \beta_{11}\tilde{x} + 2\beta_{12}\tilde{x}\tilde{y} + 3\beta_{13}\tilde{x}\tilde{y}^2 \\ &+ \beta_{21}\tilde{x}^2 + 2\beta_{22}\tilde{x}^2\tilde{y} + 3\beta_{23}\tilde{x}^2\tilde{y}^2 \\ &+ \beta_{31}\tilde{x}^3 + 2\beta_{32}\tilde{x}^3\tilde{y} + 3\beta_{33}\tilde{x}^3\tilde{y}^2.\end{aligned} \tag{14}$$

Evaluation and Results

After implementing these new refinements into a DIC software algorithm, the method was tested. The purpose of the initial tests was to determine the algorithm's capability to extract known deformation parameters from a set of images. All the images used for evaluating the method were eight-bit gray-scale bitmap images. The subset region used in the evaluations consisted of a square 41×41 pixel area centered about the node being analyzed. Theoretical images were generated to eliminate having to assess the instrumentation errors that could vary from one setup to another.

Linear Deformation Test

To evaluate the usefulness and accuracy of these new refinements, several test images were prepared. For the first test, a simple paint program was used to translate and rotate a typical random, speckle pattern image. Figure 3 shows the reference image, the translated image and the rotated image. These translated and rotated images were used to test the mapping parameters U_0, V_0, U_x, V_x, U_y and V_y, as well as the rigid-body rotation θ. Table 1 shows the results of DIC using these images. In the "percentage error" column, a blank space indicates that the percentage error is meaningless when the "exact value" is zero.

From these results, it can be seen that the new refinements to the algorithm maintain the accuracy of the previous method for purely linear displacement functions. Conservatively, the translation terms can be resolved to within ± 0.005 pixels and the rigid-body rotations to within ± 0.005 deg. The first-order displacement gradients can be determined to within ± 0.0002 and, so far, the second-order terms to within ± 0.0002 per pixel.

Second-order Deformation Test

Theoretical images with second-order deformations were created with a program that generates a new "reference" image from a sample image. The sample image would be the deformed image of the new image set and the prescribed deformation from the generated reference image. The program used the second-order displacement functions to map the pixel locations in the reference image to a location in the deformed image. The gray-scale value for each pixel in the generated reference image was then determined using bicubic spline interpolation from the mapped location in the sample image. Figure 4 shows the images used for the two second-order deformation tests. These images were analyzed, and the results are summarized in Table 2.

Again, the new refinements were able to measure the second-order displacement gradients conservatively to within ± 0.0002 per pixel. The exact theoretical principal strains for case 1 should be $\varepsilon_1 = 0.050$ and $\varepsilon_2 = 0.025$, and for case 2 should be $\varepsilon_1 = 0.050$ and $\varepsilon_2 = -0.025$. The corresponding principal strains for this displacement field at the origin were calculated to be $\varepsilon_1 = 0.04999$ and $\varepsilon_2 = 0.02501$ for case 1 and $\varepsilon_1 = 0.04966$ and $\varepsilon_2 = -0.02466$ for case 2. These tests show that the new refinements in the DIC can accurately measure the displacements and the displacement gradients of a prescribed second-order deformation field.

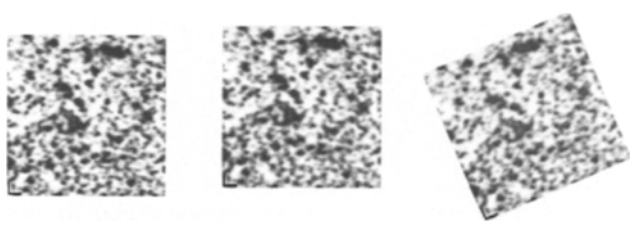

Fig. 3—Speckle pattern image translated $U = V = 12.5$ pixels and rotated 23.45 deg counterclockwise

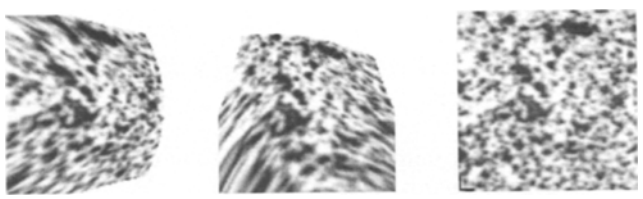

Case 1 Reference Image Case 2 Reference Image Deformed Image

Fig. 4—Images used for higher order tests

TABLE 1—RESULTS OF FIRST-ORDER DISPLACEMENT FUNCTION

Parameter	Exact Value	Measured Value	Difference	Percentage Error
Translated Image				
U_0 (pixel)	12.5	12.497	0.003	0.02
V_0 (pixel)	12.5	12.499	0.001	0.008
U_x	0.0	0.00001	0.00001	
V_x	0.0	−0.00002	0.00002	
U_y	0.0	0.00006	0.00006	
V_y	0.0	0.00001	0.00001	
U_{xx} (1/pixel)	0.0	0.00001	0.00001	
V_{xx} (1/pixel)	0.0	−0.00001	0.00001	
U_{yy} (1/pixel)	0.0	0.00001	0.00001	
V_{yy} (1/pixel)	0.0	0.00001	0.00001	
U_{xy} (1/pixel)	0.0	0.00001	0.00001	
V_{xy} (1/pixel)	0.0	0.00000	0.00000	
θ	0.0	0.0006	0.0006	
Rotated Image				
U_x	−0.08259	−0.08268	0.00009	0.01
V_x	0.39795	0.39793	0.00002	0.005
U_y	−0.39795	−0.39799	0.00004	0.01
V_y	−0.08259	−0.08262	0.00003	0.04
U_{xx}(1/pixel)	0.0	−0.00001	0.00001	
V_{xx}(1/pixel)	0.0	0.00001	0.00001	
U_{yy}(1/pixel)	0.0	0.00001	0.00001	
V_{yy}(1/pixel)	0.0	0.00002	0.00002	
U_{xy}(1/pixel)	0.0	0.00000	0.00000	
V_{xy}	0.0	0.00000	0.00000	
θ	23.450	23.452	0.002	.009

TABLE 2—RESULTS OF SECOND-ORDER DEFORMATION FUNCTION

Parameter	Exact Value	Measured Value	Difference	Percentage Error
Case 1				
U_0 (pixel)	0.0	0.001	0.001	
V_0 (pixel)	0.0	−0.0004	0.0004	
U_x	0.05	0.04999	0.00001	0.02
V_x	0.0	0.00002	0.00002	
U_y	0.0	0.00000	0.00000	
V_y	0.025	0.02501	0.00001	0.04
U_{xx} (1/pixel)	0.0075	0.00749	0.00001	0.13
V_{xx} (1/pixel)	0.0	0.00000	0.00000	
U_{yy} (1/pixel)	0.015	0.01499	0.00001	0.07
V_{yy} (1/pixel)	0.0	0.00000	0.00000	
U_{xy} (1/pixel)	0.0	0.00000	0.00000	
V_{xy} (1/pixel)	0.005	0.00500	0.00000	0
Case 2				
U_0 (pixel)	0.0	0.00031	0.00031	
V_0 (pixel)	3.5	3.5005	0.0005	0.014
U_x	0.0	−0.00004	0.00004	
V_x	0.04	0.04001	0.00001	0.025
U_y	0.03	0.02997	0.00003	0.1
V_y	0.025	0.02501	0.00001	0.04
U_{xx}(1/pixel)	0.0	0.00000	0.00000	
V_{xx}(1/pixel)	0.01	0.01000	0.00000	0
U_{yy}(1/pixel)	0.0	0.00000	0.00000	
V_{yy}(1/pixel)	0.008	0.00799	0.00001	0.13
U_{xy}(1/pixel)	0.0075	0.00750	0.00000	0
V_{xy}(1/pixel)	0.0045	0.00450	0.00000	0

As a comparison, the results of these second-order displacement field cases without accounting for the second-order displacement gradients are shown in Table 3.

The calculated principal strains are $\varepsilon_1 = 0.03734$ and $\varepsilon_2 = 0.00198$ for case 1 and $\varepsilon_1 = 0.00110$ and $\varepsilon_2 = -0.01154$ for case 2. Without the refinements in the correlation method, the first-order displacement gradients are clouded by the higher order gradients. These test results show that by measuring and accounting for the higher order gradients, the first-order gradients can be measured more accurately. The strains are calculated directly from these first-order gradients exclusively.

TABLE 3—RESULTS OF SECOND-ORDER DISPLACEMENTS WITHOUT REFINEMENTS

Parameter	Exact Value	Measured Value	Difference	Percentage Error
Case 1				
U_0 (pixel)	0.0	1.244	1.244	
V_0 (pixel)	0.0	−0.196	0.196	
U_x	0.05	0.03728	0.01272	25
V_x	0.0	−0.00702	0.00702	
U_y	0.0	0.00448	0.00448	
V_y	0.025	0.00201	0.02299	92
Case 2				
U_0 (pixel)	0.0	−0.3330	0.3330	
V_0 (pixel)	3.5	4.5895	1.0895	31
U_x	0.0	−0.00986	0.00986	
V_x	0.04	0.00259	0.03741	94
U_y	0.03	0.00601	0.02399	80
V_y	0.025	−0.00058	0.02558	102

Simulated Second-order Deformation

In the next test case, second-order deformation was simulated by acquiring images of a 22.23 mm diameter cylinder as it is rotated around its axis. This part of simulation was performed to validate the refined technique when measuring the second-order deformations only; the simulation presented here is not designed as an approach for the measurement of surface deformations of a cylindrical specimen. For measurements of surface strains on a cylindrical specimen, other methods, such as the one developed by Lu, Knauss and Vendroux,[12] can be used.

In this test, the cylinder sample was mounted vertically in an indexing head that had graduations every $\frac{3}{11}$ deg. The image acquisition system uses a Kodak Mega Plus II digital CCD camera possessing a spatial resolution of 1000 × 1000 pixels and 10-bit gray-scale. The CCD camera was placed approximately five feet from the sample, and images were acquired at various rotation angles. The images can be considered as the projection of the cylinder onto an observation plane (imaging plane). Figure 5 shows a diagram of the projection of the curved cylindrical surface onto the flat imaging plane. The values for the theoretical displacement gradients are derived under the condition that the initial point is located at the center of the image and lined up on the cylinder axis. The derivation of U_x and U_{xx} is based on two additional points located some angle φ on each side of the initial point. The distance as projected onto the imaging plane between the two points in the initial position is $d_0 = 2r\sin\varphi$ and in the rotated position is $d_r = r\sin(\theta + \varphi) - r\sin(\theta - \varphi)$. U_x is then found by taking the limit as φ approaches zero in the equation

$$U_x = \lim_{\varphi \to 0} \frac{d_r - d_0}{d_0} = \cos\theta - 1. \qquad (15)$$

The distance, as projected onto the imaging plane, of each of the two points from the initial point is $d_1 = r\sin\varphi$ and from the rotated position is $d_2 = r\sin\theta - r\sin(\theta - \varphi)$ and $d_3 = r\sin(\theta+\varphi) - r\sin\theta$. The deformation U_{xx} is then found by taking the limit as φ approaches zero in the equation

$$U_{xx} = \lim_{\varphi \to 0} \frac{\frac{d_3 - d_1}{d_1} - \frac{d_2 - d_1}{d_1}}{d_1} = -\frac{\sin\theta}{r}, \qquad (16)$$

where r is the radius of the cylinder and θ is the angle of rotation. One set of images comparing a 21 deg rotation is shown in Fig. 6. Eight different rotation angles were analyzed in this test. These angles ranged from 5.5 deg to 27 deg. Because these are actual images, other errors could be introduced, such as lighting differences around the rod,

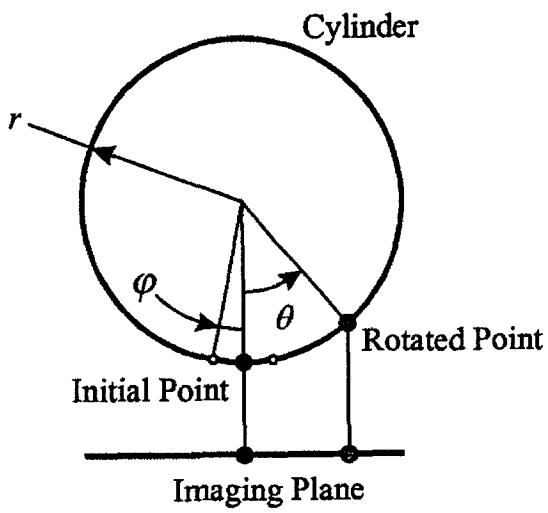

Fig. 5—Cylinder image projected onto the plane

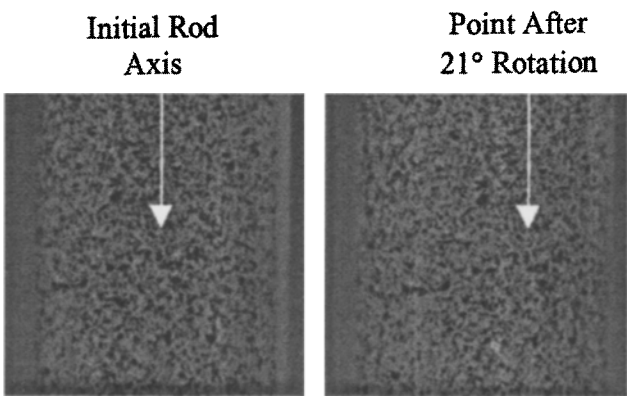

Fig. 6—Images of a cylinder rotated 21 deg

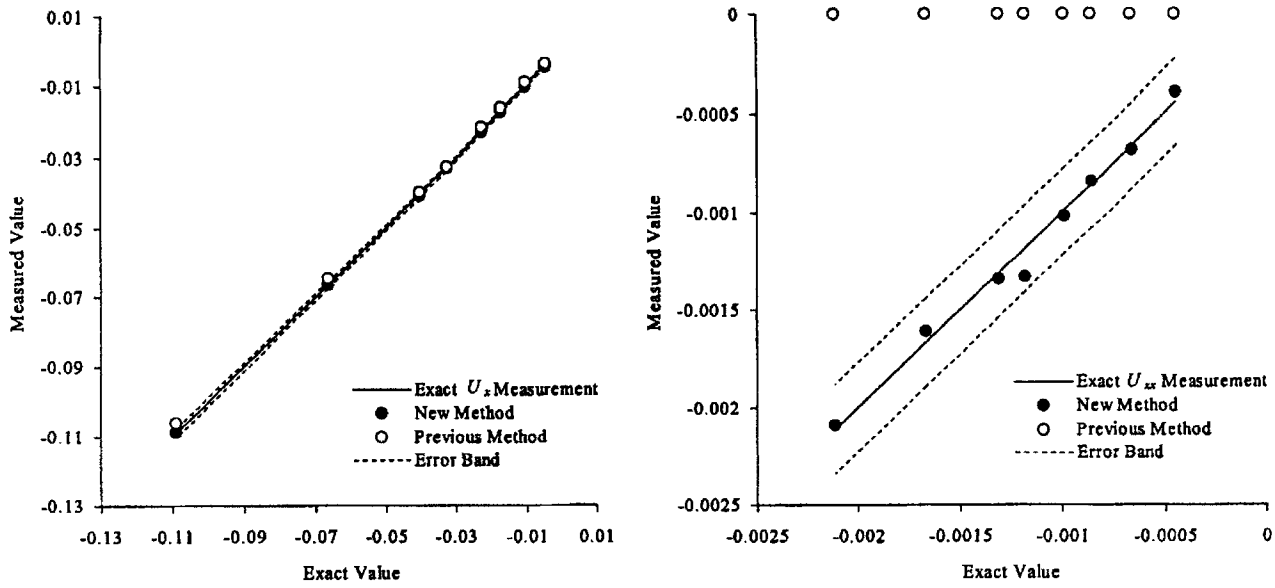

Fig. 7—Results of U_x and U_{xx} for multiple rotation angles

TABLE 4—RESULTS OF ROTATED CYLINDER TEST

Parameter	Theoretical	Measured	Difference	Percentage Error
New refined method				
U_x	−0.06642	−0.06656	0.00014	0.21
U_{xx}(1/pixel)	−0.00167	−0.00172	0.00005	3.0
Previous method				
U_x	−0.06642	−0.06458	0.00184	2.8
U_{xx}(1/pixel)	−0.00167	0	0.00167	100

measurement tolerances of the rotation angle and the camera alignment. The errors in measuring the radius of the cylinder, the prescribed rotations and the established accuracy of the new DIC method all affect the accuracy of the final measurements. The radius of the cylinder in the images was found to be 215 pixels ±2 pixels. The indexing head used to rotate the cylinder had an accuracy of $\pm\frac{3}{22}$ deg. The errors resulting from the accuracy of the prescribed angle are not constant but vary with the prescribed angle. At a nominal rotation angle of 21 deg and a cylinder radius value of 215 pixels, the expected U_x measurement would be approximately -0.066 ± 0.0009 and the expected U_{xx} measurement would be approximately −0.00167 per pixel ±0.00003 per pixel. The established accuracy of the new DIC method is ±0.0002 for the first-order deformation gradients and ±0.0002 per pixel for the second-order deformation gradients. The total error band expected in the measurement of U_x is ±0.0011 and for the measurement of U_{xx} is ±0.00023 per pixel. Figure 7 shows the exact theoretical solution as the solid diagonal line and the expected error band between the two dashed lines. The solid circles are the results of the new refined method, and the open circles are the results of the previous, linear deformation method. On the U_x results plot, Fig. 7 shows that the new method does give a more accurate measurement of the first-order displacement gradients. The maximum error for U_x using the previous method is 9.7 percent, whereas, incorporating the new refinements, the maximum error is only 1.7 percent. On the plot showing the U_{xx} results, the new method gives accurate measurements of the second-order displacement gradients whereas the previous method gave no results at all. Table 4 compares the results of the measurements at a rotation of 21 deg with the new refined DIC method and the previous method. Again, these results show the validity and accuracy of the new DIC refinements for higher order deformation.

Conclusions

The refinements to the DIC method outlined in this paper allow for the measurement of second-order displacement gradients, which provides a more accurate method of measuring the strains of materials undergoing relatively large deformation. These second-order displacement gradients can be measured by assuming a second-order approximating function for the displacement fields of the material. Measuring and isolating the higher order displacement gradients U_{xx}, V_{xx}, U_{yy}, V_{yy}, U_{xy} and V_{xy} allows for the displacement gradient components U_x, V_x, U_y and V_y, which directly contribute to the strains, to be more accurately measured in situations where higher order deformation occurs. The actual values measured for the higher order terms are not used for any of our current research on simple materials in which stress does not depend on second- or higher order displacement gradients, but could be used directly in new fields of study that depend on these higher order displacement gradients, such as gradient plasticity. The new refinements provide the same

accuracy as the previous DIC method of about ±0.0002 for the first-order displacement gradients in small-deformation conditions. These new refinements maintain that same accuracy as the deformations in the material increase, whereas the previous method would begin to lose accuracy as the higher order displacement gradients begin to cloud its measurements. More research can be done to determine whether even higher order displacement functions provide any added benefits to the method with respect to the additional computational requirements.

The DIC method for strain measurement has already been established as an effective noncontact measurement method for determining strains in a specimen. These refinements allow the DIC method to be accurately used for a more general class of deformation situations.

Acknowledgments

The authors acknowledge the support of the National Science Foundation (9872350).

References

1. Peters, W.H. and Ranson, W.F., "Digital Imaging Techniques in Experimental Stress Analysis," Opt. Eng., **21**, *427–432 (1982).*

2. Sutton, M.A., Wolters, W.J., Peters, W.H., Ranson, W.F., and McNeil, S.R., "Determination of Displacements Using an Improved Digital Image Correlation Method," Image Vision Computing, **1** *(3), 133–139 (1983).*

3. Sutton, M.A., Cheng, M., Peters, W.H., Chao, Y.J., and McNeil, S.R., "Application of an Optimized Digital Image Correlation Method to Planar Deformation Analysis," Image Vision Computing, **4** *(3), 143–150 (1986).*

4. Bruck, H.A., McNeil, S.R., Sutton, M.A., and Peters, W.H., "Digital Image Correlation Using Newton-Raphson Method of Partial Differential Correction," EXPERIMENTAL MECHANICS, **29**, *261–267 (1989).*

5. Luo, P.F., Chao, Y.J., Sutton, M.A., and Peters, W.H., "Accurate Measurement of Three-dimensional Deformations in Deformable and Rigid Bodies Using Computer Vision," EXPERIMENTAL MECHANICS, **33**, *123–132 (1993).*

6. Vendroux, G. and Knauss, W.G., "Submicron Deformation Field Measurements: Part 1. Developing a Digital Scanning Tunneling Microscope," EXPERIMENTAL MECHANICS, **38**, *18–23 (1998).*

7. Vendroux, G. and Knauss, W.G., "Submicron Deformation Field Measurements: Part 2. Improved Digital Image Correlation," EXPERIMENTAL MECHANICS, **38**, *86–91 (1998).*

8. Vendroux, G. and Knauss, W.G., "Submicron Deformation Field Measurements: Part 3. Demonstration of Deformation Determinations," EXPERIMENTAL MECHANICS, **38**, *154–160 (1998).*

9. Vendroux, G., "Correlation: A Digital Image Correlation Program for Displacement and Displacement Gradient Measurements," GALCIT Report No. SM90-19, California Institute of Technology (1990).

10. Späth, H., Two Dimensional Spline Interpolation Algorithms, AK Peters, Wellesley, MA (1995).

11. Gerald, C.F. and Wheatley, P.O., Applied Numerical Analysis, Addison-Wesley, Reading, MA (1994).

12. Lu, H., Knauss, W.G., and Vendroux, G., "Surface Deformation Measurements of a Cylindrical Specimen by Digital Image Correlation," EXPERIMENTAL MECHANICS, **37**, *433–439 (1997).*